RSC Advances

ROYAL SOCIETY OF CHEMISTRY

www.rsc.org/advances

The effects of main components of seawater on the tribological properties of Cu-9Al-5Ni-4Fe-Mn alloy sliding against AISI 52100 steel

Kongjie Jin [a, b], Zhuhui Qiao [a, *], Shuai Wang [a, b], Shengyu Zhu [a], Jun Cheng [a], Jun Yang [a], Weimin Liu [a]

a State Key Laboratory of Solid Lubrication, Lanzhou Institute of Chemical Physics, Chinese Academy of Sciences, Lanzhou 730000, PR China

b University of Chinese Academy of Sciences, Beijing 100049, PR China

* Corresponding author. Tel: +86-931-4968193; fax: +86-931-8277088.

E-mail address: zhqiao@licp.cas.cn (ZH Qiao); jyang@licp.cas.cn (J Yang)

Abstract

A high strength and wear-resistance nickel-aluminum bronze alloy was successfully prepared by hot-pressing sintering. The tribological performances of it sliding against AISI 52100 steel were studied in distilled water, seawater, divalent salts solution and monovalent salts solution. The effects of main components of seawater on the tribological properties were firstly investigated. The results show that Cu-9Al-5Ni-4Fe-Mn alloy has lower friction coefficient and wear rate in seawater and divalent salts solution. The Cl^- and SO_4^{2-} adsorbed by surface can accelerate corrosion and promote the formation of Cu_2O, Al_2O_3, FeOOH and Fe_2O_3, which has an influence on the tribological performances. The distribution of $CaCO_3$ and $Mg(OH)_2$ on the surface also plays an important role in the reduction of the friction coefficient and wear rate. In addition, many substances transfer from the alloy to steel

surface and form a transfer layer during the friction process.

Keywords: Copper alloy; Seawater; Friction; Salts

1. Introduction

Cu-9Al-5Ni-4Fe-Mn alloy (henceforth referred to as CANFM alloy) is a kind of important engineering material.[1-5] It has been widely employed in marine applications,[6-8] because of the combination of superior corrosion resistance and reliability.[9-13] Recently, many works focused on the tribological characteristic of bronzes.[14-17] However, the tribological properties of CANFM alloy are relatively unknown.

Meanwhile, it has been reported that Cu-6Sn-6Zn-3Pb bronze has different tribological properties under seawater and distilled water.[18, 19] The varying content of salts in seawater has obvious influences on the tribological properties of PEEK.[20] Chen et al. also reported that polymers exhibit better lubricating property under seawater than pure water, because of the deposition of $CaCO_3$ and $Mg(OH)_2$ on the surface.[21] Additionally, seawater corrosion could change chemical composition and morphology of surfaces thereby influencing friction coefficient and wear rate of materials.[7, 22, 23] It is known that seawater is mainly composed of sodium salt (NaCl, Na_2SO_4), divalent metal salts ($CaCl_2$, $MgCl_2$) and monovalent metal salts. Therefore, it is necessary to study the effects of sodium salt, divalent metal salts and monovalent metal salts on the tribological properties of CANFM alloy in seawater environment.

Here, the tribological performances of CANFM alloy were investigated in distilled water, seawater and other salts solutions. The effects of divalent metal salts,

NaCl, Na_2SO_4, oxides and corrosion products on tribological properties were studied, as well as the tribocorrosion mechanisms of CANFM alloy and steel in seawater.

2. Experimental procedures

2.1. Sample preparation

The CANFM alloy consists of 9 wt.% Al, 5 wt.% Ni, 4 wt.% Fe and 1 wt.% Mn with the balance of Cu. All metal powders were mixed by Fritsch Pulverisettes 5 planetary ball-milling machine for 10 hours at a rotational speed of 170 rpm. The grinding media were WC/Co balls, and the ratio of the ball to powder was 2:1. The mixed powders were then placed in a BN-coated graphite mold, and were sintered at 860 °C with an axial pressure of 38 MPa for 15 min at a vacuum of 10^{-2} Pa. Finally, the specimens were naturally cooled to room temperature. The Vickers hardness of CANFM alloy was measured with MH-5 Vickers hardness instrument with a load of 2 N and a dwell time 10 s. The bending and compressive strengths were measured with DY-35 mechanical testing machine at ambient.

2.2. Friction and wear tests

The seawater used here was prepared according to the standard ASTM D1141-98 (2008) as listed in Table 1. The chemical components of seawater can be divided into four parts:

I. Divalent metal salts: $MgCl_2 + CaCl_2 + SrCl_2$

II. Monovalent metal salts: KCl + KBr + NaF

III. Main sodium salts: $NaCl + Na_2SO_4$

IV. Other components: $H_3BO_3 + NaHCO_3$

Table 1 Chemical compositions of seawater, solution D and solution M (g/L)

Part	Compound	Seawater	Solution D	Solution M
I	$MgCl_2$	5.200	5.200	/
	$CaCl_2$	1.160	1.160	/
	$SrCl_2$	0.025	0.025	/
II	KCl	0.695	/	0.695
	KBr	0.101	/	0.101
	NaF	0.003	/	0.003
III	NaCl	24.530	/	/
	Na_2SO_4	4.090	/	/
IV	$NaHCO_3$	0.201	0.201	0.201
	H_3BO_3	0.027	0.027	0.027

In order to study the effects of sodium salt, divalent metal salts and monovalent metal salts, solution D and solution M were prepared as listed in Table 1. Here, solution D contained divalent metal salts, and solution M contained monovalent metal salts. The contents of salts were the same as those in seawater. Meanwhile, the PH values of prepared seawater and solutions were adjusted to 8.2 by HCl solution (0.1mol/L) and NaOH solution (0.1mol/L).

Friction and wear tests were carried out using a CFT-1 reciprocating friction tester at 25 °C in distilled water, seawater, solution D and solution M. AISI 52100 bearing steel ball with the diameter of 4 mm was chosen as counterface. The hardness of AISI 52100 steel was 60 HRC, and the surface roughness (Ra) was 0.02 mm. All tests were conducted under different loads (10, 15, 20, 25 and 30 N) with 0.05 m/s sliding speed and different sliding speeds (0.017, 0.033, 0.050, 0.067 and 0.083 m/s) under 15 N load for 30 min. The wear rate (W) was calculated by the equation $W=V/SP$ in which V is wear volume, S is sliding distance (m) and P is applied load (N). The wear volume (V) was measured with Micro Xam-3D surface profiler. Each friction coefficient and wear rate in this paper represents the average value of four

tests under the same testing parameters.

2.3. Sample characterization

The X-ray diffractometer (XRD, D/max-2400, Japan) was used to identify the phase constituents of the alloy. Microstructural characterization was performed with scanning electron microscopy (SEM, JSM-5600LV). The energy dispersive spectroscopy (EDS, Kevex) was used to detect the chemical composition of the worn surfaces. The chemical states of the elements on the worn surfaces were examined by a PHI-5702 multifunctional X-ray photoelectron spectroscope (XPS). Moreover, a laser Raman spectrometer (Renishaw inVia) was used to analyze the worn surfaces.

3. Results and discussion

3.1. Material characterization

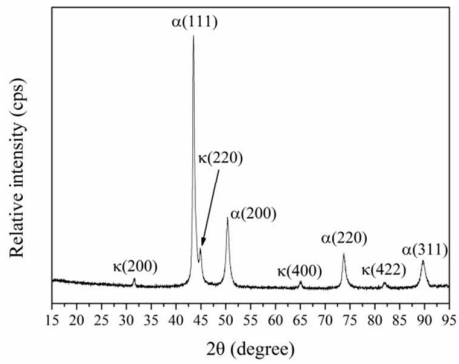

Fig. 1 XRD pattern of the hot-pressed sintering CANFM alloy.

The X-ray diffraction (XRD) pattern of the sintered CANFM alloy is given in Fig. 1. The main phases consist of α phase (Cu-rich, fcc crystal structure) and κ-phase precipitates (Ni-Fe-Al complex).[24] Meanwhile, the density and mechanical properties of prepared alloy are listed in Table 2.

Table 2 Density and mechanical properties of the CANFM alloy

Material	Density (g/cm^3)	Hardness (HV)	Compressive strength (MPa)	Bending strength (MPa)

CANFM alloy	7.42	170.4	1049.2	811.3

3.2. Friction and wear properties

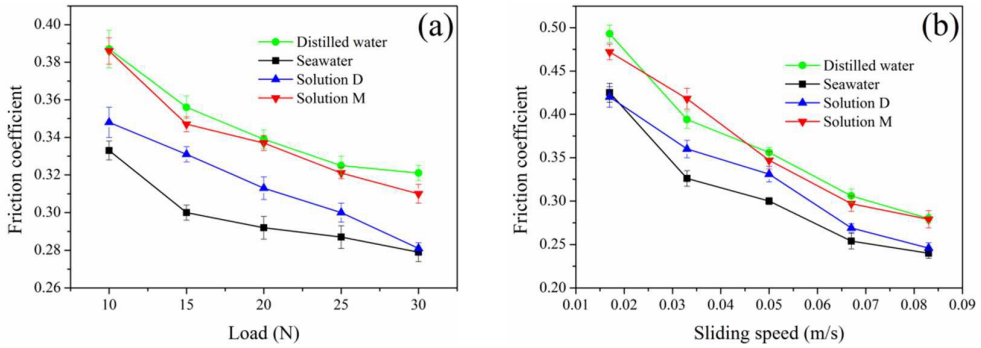

Fig. 2 Friction coefficient of CANFM alloy at different loads (a) and different sliding speeds (b) in distilled water, seawater, solution D and solution M.

Fig. 2 shows the friction coefficients of CANFM alloy with various loads at 0.05 m/s and various sliding speeds under 15 N in the four liquids. The results are as follows:

(A) In distilled water and solution M, friction coefficients are the highest;

(B) Under the same testing parameters, friction coefficients in solution D are lower than those in solution M;

(C) Friction coefficients of CANFM alloy are the lowest in seawater.

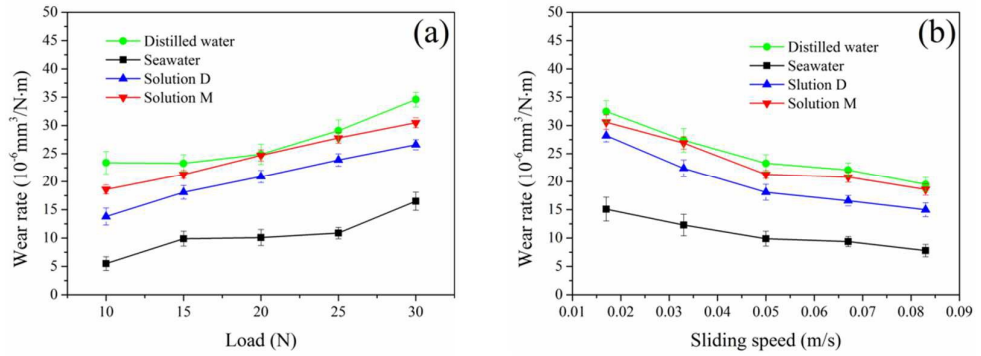

Fig. 3 Wear rate of CANFM alloy at different loads (a) and different sliding speeds (b) in distilled water, seawater, solution D and solution M.

The wear rates of CANFM alloy under various loads at 0.05m/s and various sliding speed at 15 N in the four liquids are given in Fig. 3. The results can be

concluded as follows:

(a) In distilled water and solution M, wear rates are the highest;

(b) Wear rates of CANFM alloy in solution D are lower than those in solution M;

(c) The wear rates are the lowest in seawater.

The above results reveal that CANFM alloy has different tribological performances in distilled water, seawater, solution D and solution M. Divalent metal salts (part I in Table 1), NaCl and Na_2SO_4 (part III in Table 1) are the key factors for the decrease of friction coefficients and wear rates.

3.3. Characterization of the worn surface of CANFM alloy

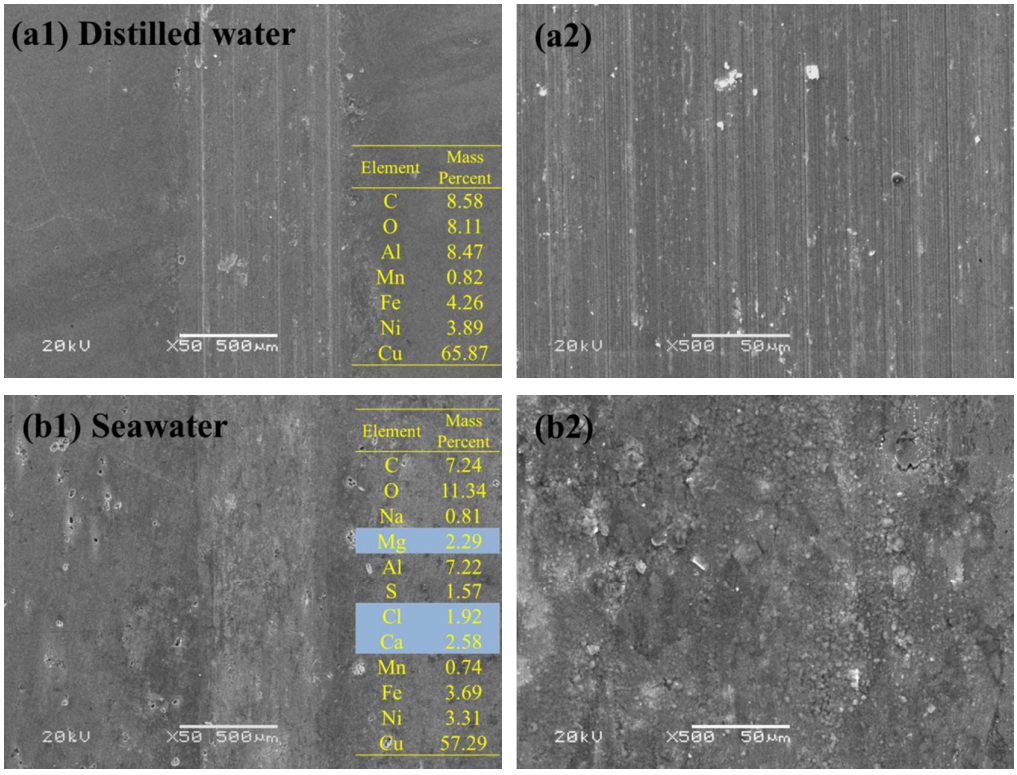

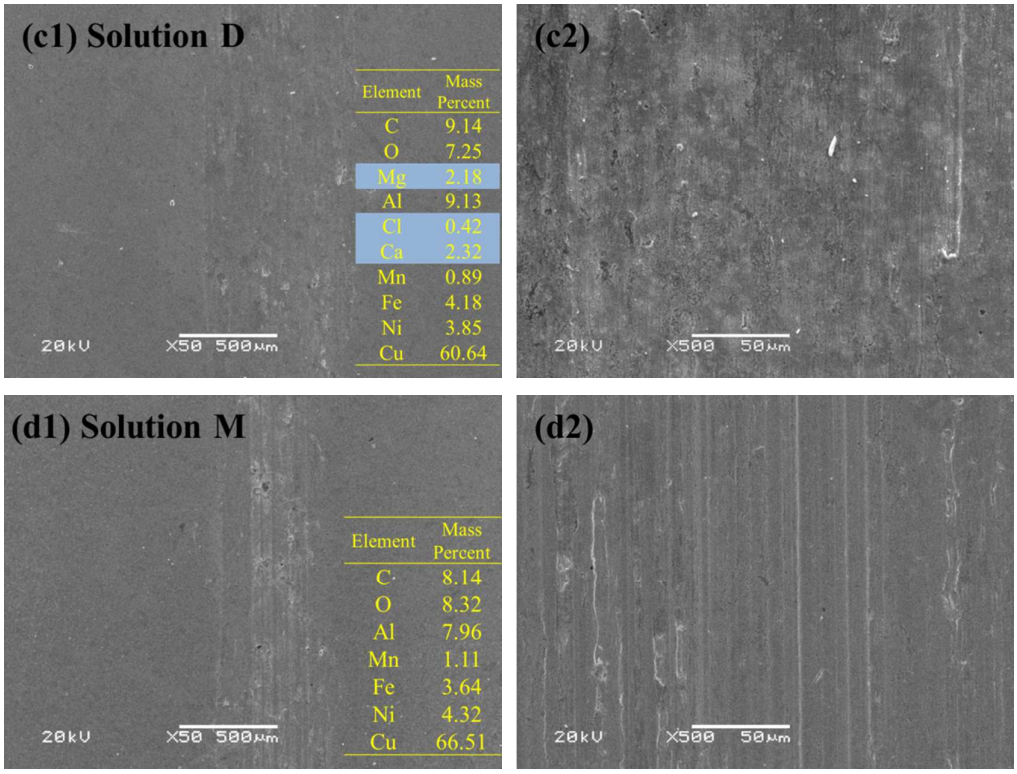

Fig. 4 SEM images of the worn surfaces on CANFM alloy after sliding in distilled water (a1, a2), seawater (b1, b2), solution D (c1, c2) and solution M (d1, d2) at 15 N and 0.05 m/s.

Fig. 4 shows SEM images of the worn surfaces of CANFM alloy in the four liquids. The wear scar and enlarged view are given simultaneously. In distilled water (Figs. 4a1 and a2), the worn surface suffers more severe worn compared with other solutions. There are a lot of grooves paralleling to sliding direction on the worn surface. In seawater (Figs. 4b1 and b2) and solution D (Figs. 4c1 and c2), fewer grooves form on the worn surfaces. Many wear debris and mixtures deposit on the surface in seawater. In solution M (Figs. 4d1 and d2), as in distilled water, many shallow grooves can be observed. The above analyses indicate that the wear of CANFM alloy in seawater and solution D is milder than it in distilled water and solution M. It corresponds to the experimental results that CANFM alloy has lower friction coefficient and wear rate in seawater and solution D (Figs. 2 and 3).

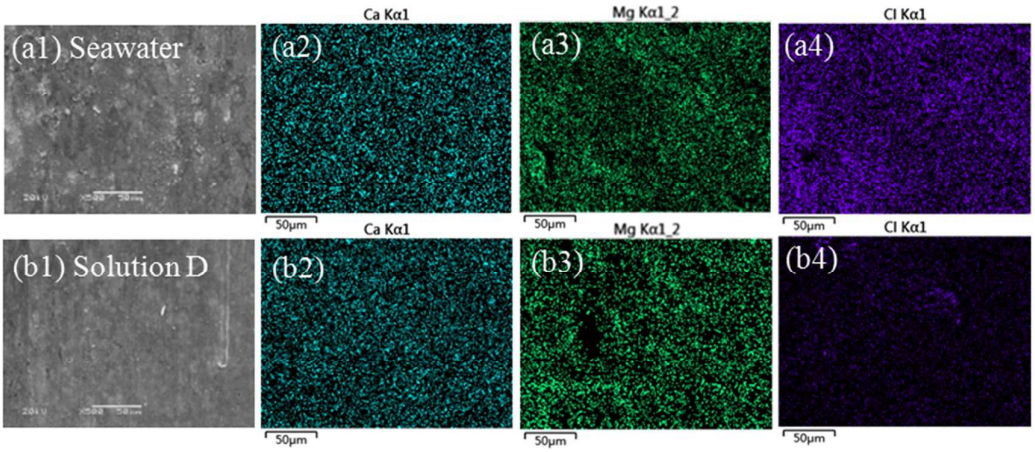

Fig. 5 Elemental mapping of Ca, Mg and Cl on the worn surfaces of CANFM alloy in seawater (a1-a4) and solution D (b1-b4).

Meanwhile, the EDS analysis (Fig. 4) shows that some amounts of Ca, Mg and Cl are detected on the worn surfaces in seawater and solution D. As shown in elemental mapping (Fig. 5), Ca, Mg and Cl distribute uniformly on the worn surfaces. It is known that most metal surfaces contain oxides that strongly adsorb various ions. Thus, large amounts of Ca^{2+}, Mg^{2+} and Cl^{-} are adsorbed on the alloy surfaces during the friction testing.

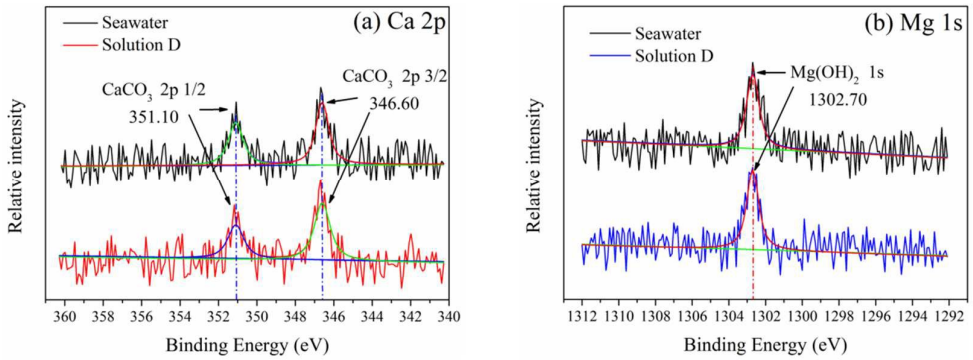

Fig. 6 XPS spectrums of Ca (a) and Mg (b) elements on the worn surfaces of CANFM alloy after sliding in seawater and solution D.

Fig. 6 gives the XPS spectrums of Ca and Mg on the worn surfaces after sliding in seawater and solution D. As shown in Fig. 6a, the peaks at 351.10 eV (Ca 2p 1/2) and 346.60 eV (Ca 2p 3/2) are assigned to $CaCO_3$.[25, 26] In Fig. 6b, the peak of Mg 1s

at 1302.70 eV is assigned to $Mg(OH)_2$.[27] During the friction process in seawater, various ions including Ca^{2+}, Mg^{2+}, OH^-, $HCO_3^-$and CO_3^{2-} are adsorbed on the steel surface. Some of them react with each other and produce $CaCO_3$ and $Mg(OH)_2$.[20, 21, 28] Then, $CaCO_3$ and $Mg(OH)_2$ are adsorbed on the surface and form the weakly-bound surface layer. It has been investigated that the distribution of $CaCO_3$ and $Mg(OH)_2$ can prevent the wear surfaces from direct contact, leading to a decrease of the plowing effect. Besides, $CaCO_3$ and $Mg(OH)_2$ form the mixed film with some lubricating effect together with wear debris.[20, 21, 29]

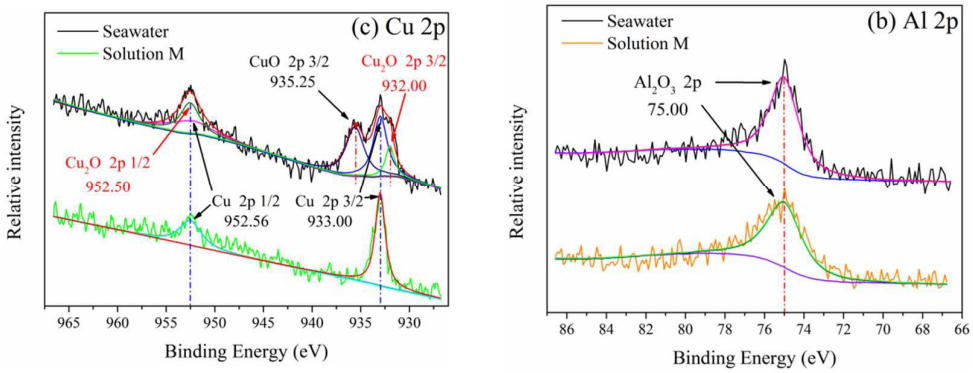

Fig. 7 XPS spectrums of Cu (a) and Al (b) on the worn surfaces of CANFM alloy after sliding in seawater and solution M.

In addition, the XPS spectrums of Cu on the worn surfaces in seawater and solution M are given in Fig. 7a. In seawater, the peak at 935.25 eV (Cu 2p 3/2) is associated with CuO.[30] The peaks at 952.50 eV (Cu 2p 1/2) and 932.00 eV (Cu 2p 3/2) are assigned to Cu_2O.[31-33] In aerated chloride media, the main corrosion process of bronze is the dissolution of copper to form the dichlorocuprous anion complex ($CuCl_2^-$) and oxide (Cu_2O).[32, 34] The reaction process is generally simplified as follows:[22, 35]

$$Cu + 2Cl^- \rightarrow CuCl_2^- + e^-$$

$O^2 + 2H_2O + 4e^- \rightarrow 4OH^-$

$2CuCl_2^- + 2OH^- \rightarrow Cu_2O + H_2O + 4Cl^-$

Meanwhile, it has been reported that the cupric complexes in MCl solution (M: Na^+, K^+, Ca^+, Mg^+) may form a series of hydrate clusters $[CuCl_n(H_2O)_m]^{2-n}$ (n=1-4). The various concentrations of cupric complexes can change the coordination number of hydrate clusters thereby affecting the chemical and physical properties of the solution.[36-39] Nevertheless, it is not clear whether this process has an influence on the tribological performance of CANFM alloy. Further work is required to verify this assumption, which will be done in our next stage.

Moreover, Fig. 7b gives the XPS spectrums of Al on the worn surfaces in seawater and solution M. Two curves have the same peaks at 75.00 eV (Al 2p) which is assigned to Al_2O_3. It indicates that Al_2O_3 form on the surface in seawater and solution M. It has been reported that the Al_2O_3 film on the surface can protect alloy against the corrosion effect of solutions.[12, 23]

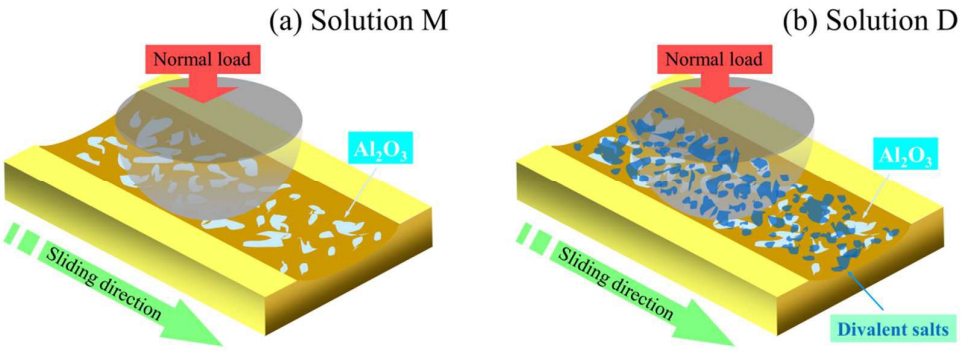

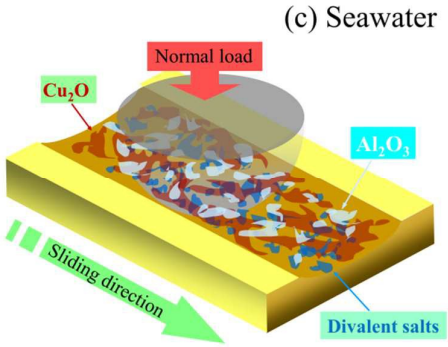

Fig. 8 Schematic diagrams of worn surfaces of CANFM alloy in solution M (a), solution D (b) and seawater (c).

In conclusion, the worn surfaces of CANFM alloy in the different solutions can be described schematically in Fig. 8. In solution M, the compound on the worn surface is mainly Al_2O_3. In solution D, $CaCO_3$ and $Mg(OH)_2$ form on the surface together with Al_2O_3. In seawater, high concentration of Cl^- can accelerate the corrosion and promote the formation of Cu_2O on the surface.[40, 41] Thus, in seawater environment, Al_2O_3, $CaCO_3$, $Mg(OH)_2$ and Cu_2O adsorb on the surface and form the weakly-bound surface layers.[42-44]

3.4. Characterization of the worn surface of steel counterface

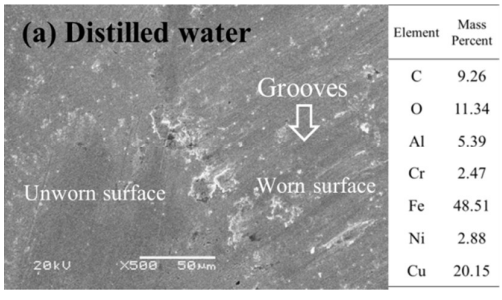

Element	Mass Percent
C	9.26
O	11.34
Al	5.39
Cr	2.47
Fe	48.51
Ni	2.88
Cu	20.15

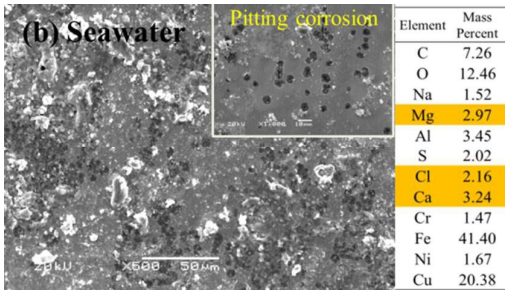

Element	Mass Percent
C	7.26
O	12.46
Na	1.52
Mg	2.97
Al	3.45
S	2.02
Cl	2.16
Ca	3.24
Cr	1.47
Fe	41.40
Ni	1.67
Cu	20.38

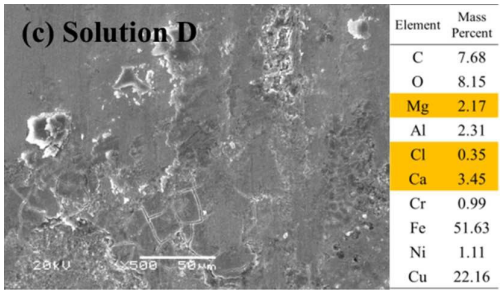

Element	Mass Percent
C	7.68
O	8.15
Mg	2.17
Al	2.31
Cl	0.35
Ca	3.45
Cr	0.99
Fe	51.63
Ni	1.11
Cu	22.16

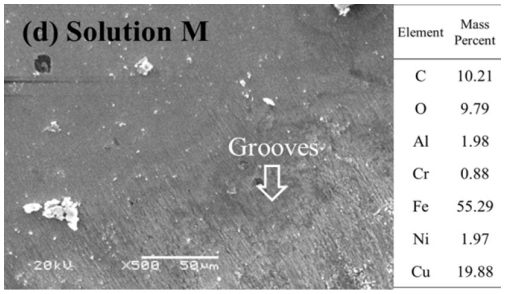

Element	Mass Percent
C	10.21
O	9.79
Al	1.98
Cr	0.88
Fe	55.29
Ni	1.97
Cu	19.88

Fig. 9 SEM images of wear scars on steel ball after sliding in distilled water (a), seawater (b), solution D (c) and solution M (d) at 15 N and 0.05 m/s.

Fig. 9 shows SEM images of the worn surfaces of steel after sliding in the four liquids (15 N, 0.05 m/s). In distilled water (Fig. 9a) and solution M (Fig. 9d), the worn surfaces are similar that many parallel grooves are observed. In seawater (Fig. 9b), pitting corrosion occurs on the worn surface, because of the high concentration of Cl^- in seawater corrosion. Cl^- ions are known to adsorb strongly and to modify iron, aluminum and other oxide layers, with a strong effect on metal corrosion. In solution D (Fig. 9c), pitting corrosion does not occur, and minor amount of Ca and Mg elements are detected as the surface in seawater.

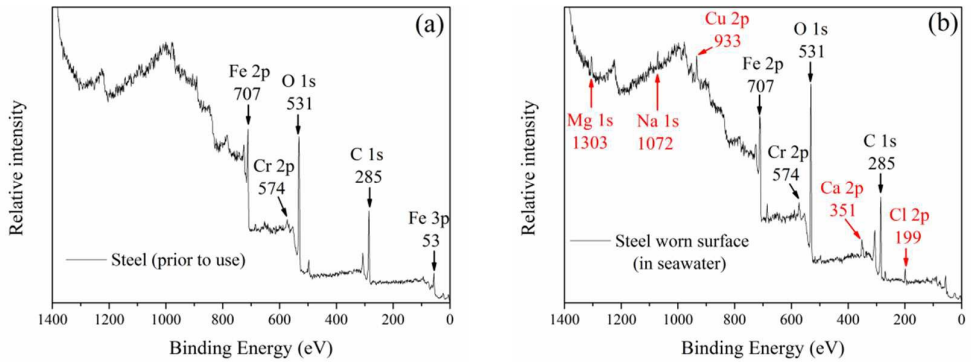

Fig. 10 XPS survey spectrums of steel surface (prior to use) (a) and worn surface after sliding in seawater (b).

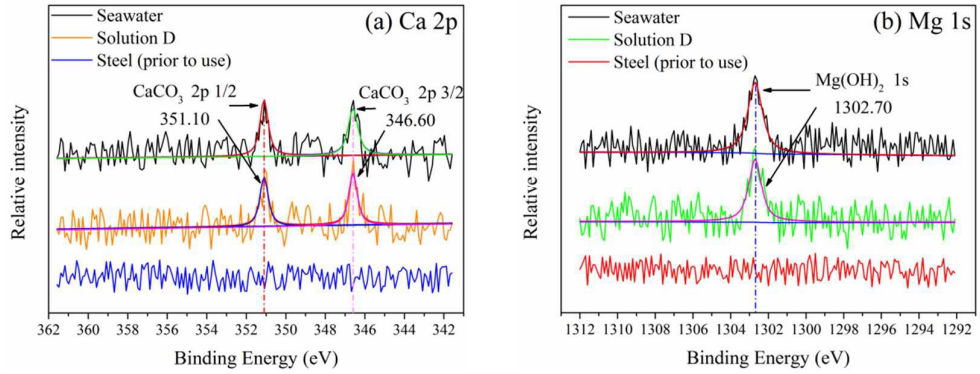

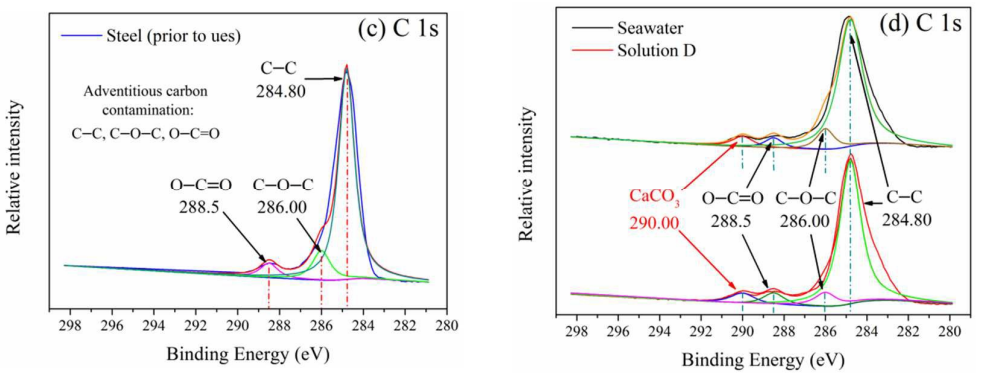

Fig. 11 XPS spectrums of Ca (a) and Mg (b) on the worn surfaces generated in seawater and solution D, as well as the steel surface (prior to use). XPS spectrums of C on the steel surface (prior to use) (c) and worn surfaces generated in seawater and solution D (d).

Figs. 10a and b give the XPS survey spectrums of steel (prior to use) and worn surface generated in seawater. It can be seen that Mg, Na, Ca, Cl and Cu are detected on the worn surface. It is well known that, during the friction process in seawater, most metal surfaces contain oxides that strongly adsorb various ions. In this process, the Ca^{2+}, Mg^{2+}, OH^-, $HCO_3^-$and CO_3^{2-} react with each other and produce $CaCO_3$ and $Mg(OH)_2$ on the surface.[20, 21, 28] The reaction process is generally simplified as follows:

$$Mg^{2+} + 2OH^- \rightarrow Mg(OH)_2$$

$$HCO_3^- + OH^- \rightarrow CO_3^{2-} + H_2O$$

$$Ca^{2+} + CO_3^{2-} \rightarrow CaCO_3$$

As shown in Figs. 11a, the peaks at 351.10 eV (Ca 2p 1/2) and 346.60 eV (Ca 2p 3/2) are assigned to $CaCO_3$.[45-47] In Fig. 11b, the peak at 1302.70 ev (Mg 1s) is associated with $Mg(OH)_2$.[48] Furthermore, Figs. 11c and d give the XPS spectrums of C on the steel surface (prior to use) and worn surface generated in seawater and solution D. In Fig. 11c, the peaks are mainly assigned to adventitious carbon contamination (C－C, C－O－C, O－C=O). In Fig. 11d, the peak at 290.00 eV (C 1s)

is associated with $CaCO_3$.[49]

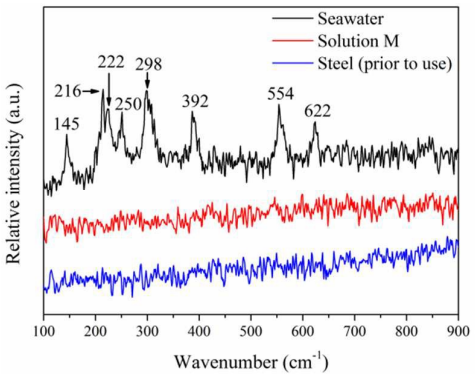

Fig. 12 Raman spectrums of steel surface (prior to use) and worn surfaces of steel generated in seawater and solution M.

As shown Fig. 12, the Raman spectrum of worn surface generated in seawater displays three peaks at 145, 216 and 622 cm^{-1}. The peak at 145 cm^{-1} is associated with Cu_2O.[50, 51] The peak at 216 cm^{-1} is attributed to Cu_2O [50, 51] or $Cu_2Cl{\cdot}2H_2O$.[52] The peak at 622 cm^{-1} might be related to the presence of Cu_2O.[51] Thus, it is very likely that Cu_2O form on the steel surface.

Meanwhile, the Raman spectrum of worn surface generated in seawater displays the other five peaks. The peak at 250 cm^{-1} is assigned to α-FeOOH [53] or γ-FeOOH.[54, 55] The peak at 392 cm^{-1} is associated with α-FeOOH [55, 56] or γ-FeOOH.[53, 54] The peak at 554 cm^{-1} could be related to the presence of α-FeOOH [54] or Fe_3O_4.[56, 57] Meanwhile, the peak at 222 cm^{-1} is assigned to α-Fe_2O_3.[53, 54, 58] The peak at 298 cm^{-1} is related with α-Fe_2O_3.[59] Thus, it can be inferred that FeOOH and Fe_2O_3 form on the steel surface in seawater environment.

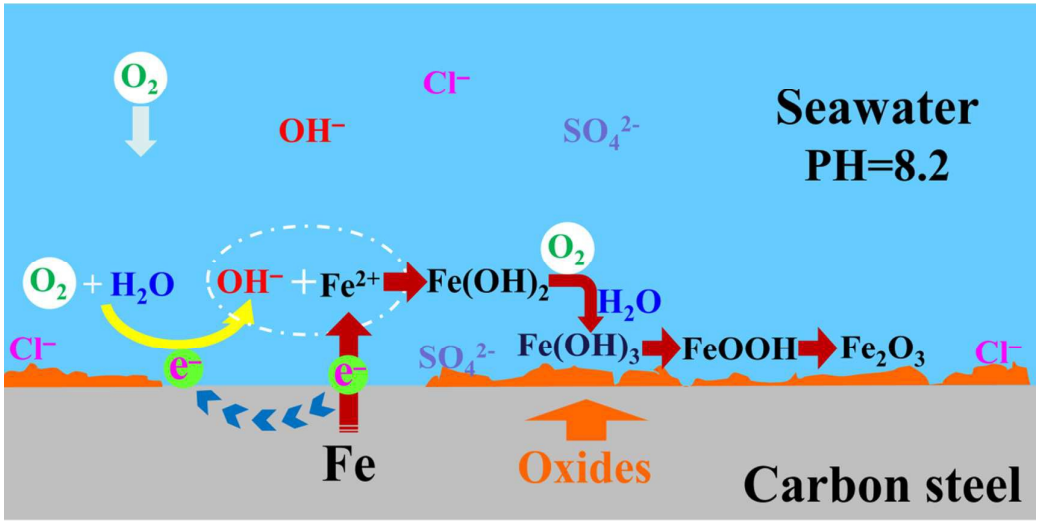

Fig. 13 Schematic diagram of the chemical state of steel surface in seawater.

The chemical state of the steel surface in seawater can be described schematically in Fig. 13. It is well known that there are lots of oxides on the surface of bearing steel. Some of them are produced by the autoxidation of original surface in air. The other oxides are produced by the electrochemical reaction of steel surface in seawater. As various elements (Fe, C, Mn, Si etc.) in bearing steel have different electrode potential, countless minute corrosive cells form on the steel surface in seawater environment. The cathodic and anodic reactions take place as follows:[54, 60]

$O^2 + 2H_2O + 4e^- \rightarrow 4OH^-$ (cathodic reaction)

$Fe \rightarrow Fe^{2+} + 2e^-$ (anodic reaction)

Cl^- and SO_4^{2-} adsorbed by surface can accelerate corrosion by promoting Fe easily dissolve as Fe^{2+}. Then, Fe^{2+} reacts with OH^- and O_2 subsequently:

$Fe^{2+} + 2OH^- \rightarrow Fe(OH)_2$

$2Fe(OH)_2 + O^2 + H_2O \rightarrow 2Fe(OH)_3$

$Fe(OH)_3 \rightarrow FeOOH + H_2O$

$2FeOOH \rightarrow Fe_2O_3 + H_2O$

Eventually, a lot of oxides (Fe_2O_3) form on the surface of bearing steel (Fig. 13). Furthermore, FeOOH and Fe_2O_3 are easily adsorbed on the surface and form the weakly-bound surface layer, which contributes to the adhesion of various ions and inorganic compounds on the surface. Then, the weakly-bound surface layer somewhat avoids the contact between the CANFM alloy and steel, and decreases the friction and wear.[61, 62] However, the weakly-bound surface layer is unstable and is easily damaged during the friction process. O_2 and Cl^- readily penetrate the layer and dissociate on the steel surface.[42-44] Thus, the weakly-bound surface layer cannot prevent the seawater corrosion.

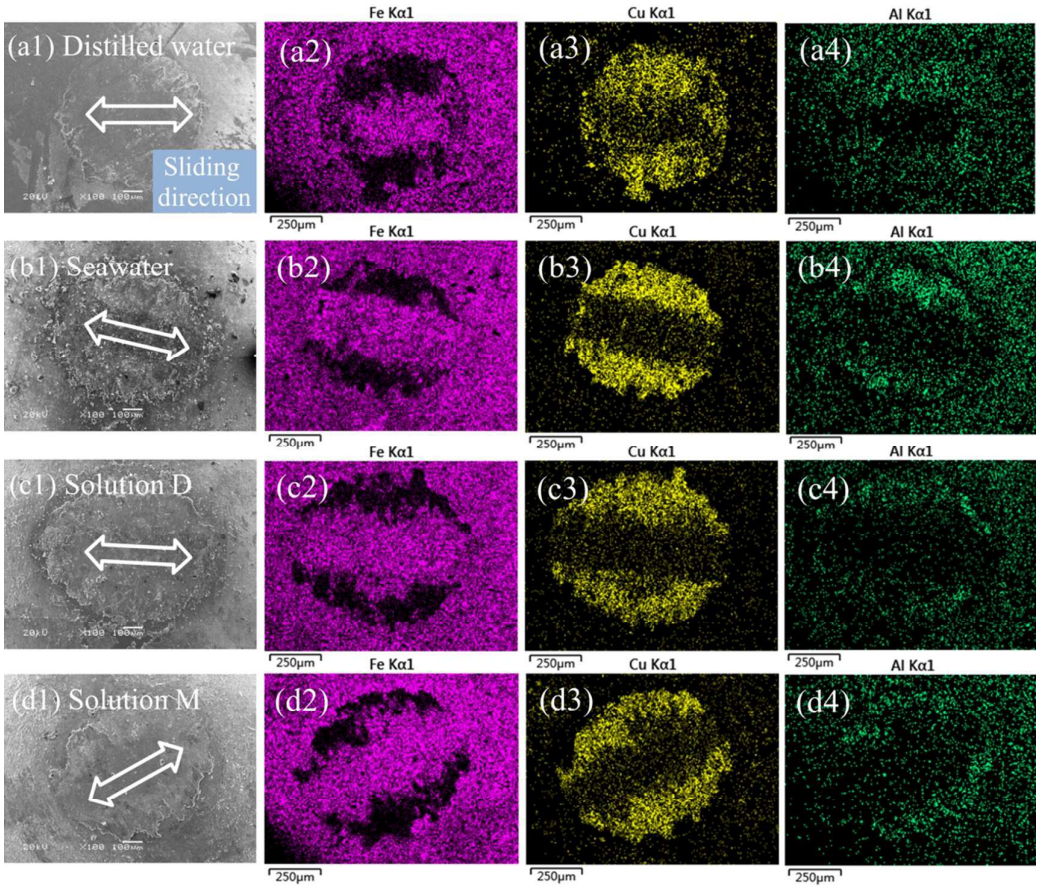

Fig. 14 Elemental mapping of Fe, Cu and Al on the worn surfaces of CANFM alloy in distilled water (a1-a4), seawater (b1-b4), solution D (c1-c4) and solution M (d1-d4).

In addition, as shown in Fig. 14, high levels of Cu and Al transfer from CANFM

alloy to the steel surface during the friction process. These transferred substances form a transfer layer which can partly separate the surface of steel from seawater.[63-65] Meanwhile, Due to the good corrosion resistance of CANFM alloy, the corrosion effect of seawater on steel can be weakened by the transfer layer.

3.5. Characterization of the surfaces immersed in the three solutions

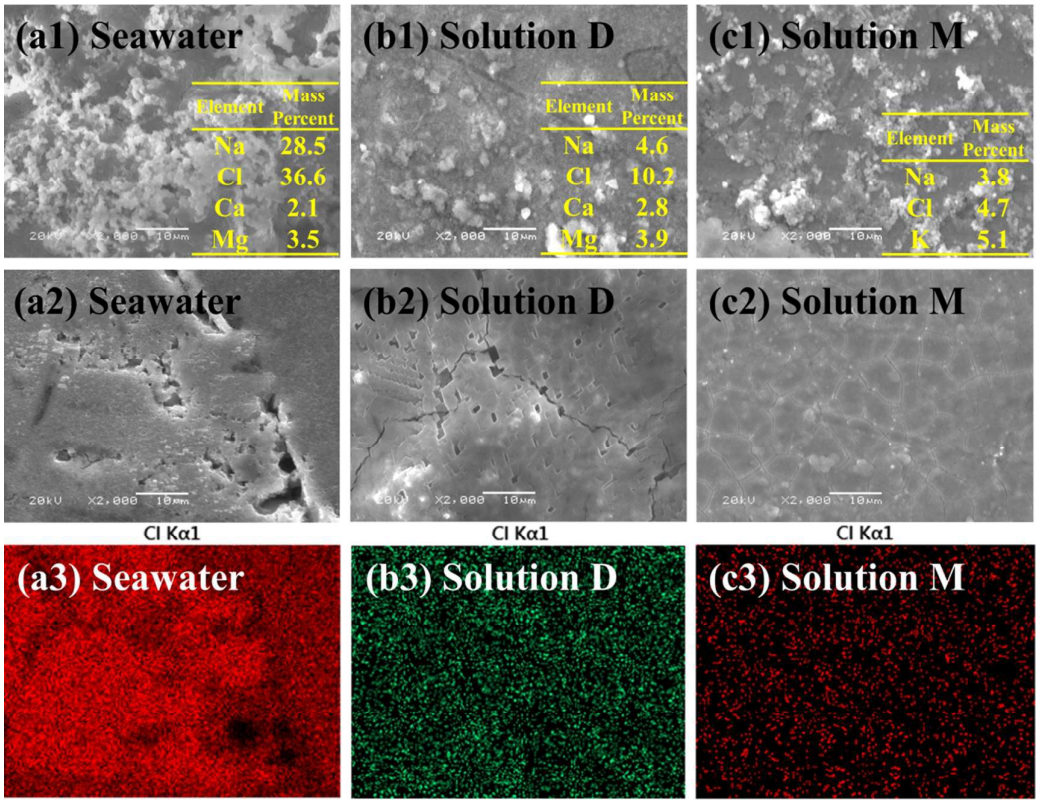

Fig. 15 SEM images of sample surfaces (a1-c1) and corroded surfaces (a2-c2) of CANFM alloy after immersed in seawater, solution D and solution M, and elemental mapping of Cl on the corroded surface (a3-c3).

The immersion corrosion tests of the CANFM alloy and bearing steel were performed in seawater, solution D and solution M. The samples were immersed into the solutions for 10 hours. Figs. 15a1-c1 show SEM images of the CANFM alloy surfaces after immersed in three solutions. As shown in Fig. 15a1, large amounts of salts mainly consisting of Na, Cl, Ca and Mg deposit on the surface generated in

seawater. These salts are produced by the evaporation of the seawater adsorbing on the surface. In Figs. 15b1 and c1, the salts depositing on the surfaces are fewer than those in seawater, because of the lower contents of salts in solution D and solution M.

In order to observe the corroded surfaces, the salts were wiped by cotton gently. As shown in Fig. 15a2, severe pitting corrosion occurs at some areas of the steel surface immersed in seawater. Meanwhile, a high level of Cl is detected on the corroded surface (Fig. 15a3). The Cl^- ions adsorbing on the surface strongly modify the alloy surface, with a strong effect on metal corrosion.

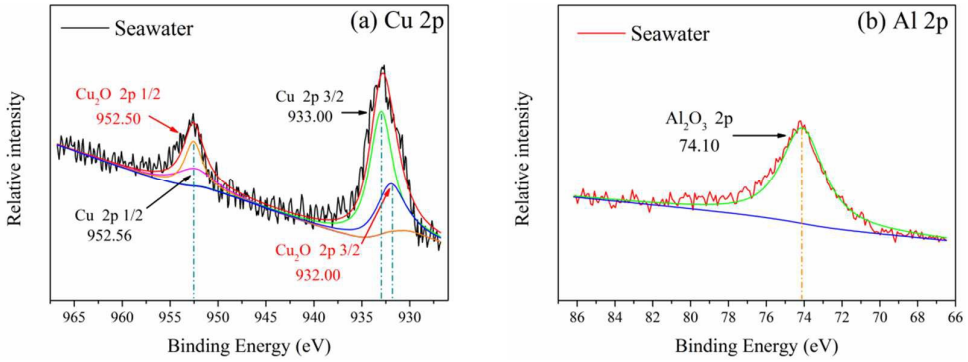

Fig. 16 XPS spectrums of Cu (a) and Al (b) on the corroded surface after immersed in seawater.

Fig. 16 gives the XPS spectrums of Cu and Al on the corroded surface after immersed in seawater. The peaks at 952.50 eV (Cu 2p 1/2) and 932.00 eV (Cu 2p 3/2) are assigned to Cu_2O (Fig. 16a).[31-33] The peak of Al 2p at 74.10 eV is associated with Al_2O_3 (Fig. 16b).[66] The existence of Cu_2O and Al_2O_3, main corrosion produces of CANFM alloy in seawater, indicates that the alloy surface is severely corroded by seawater.

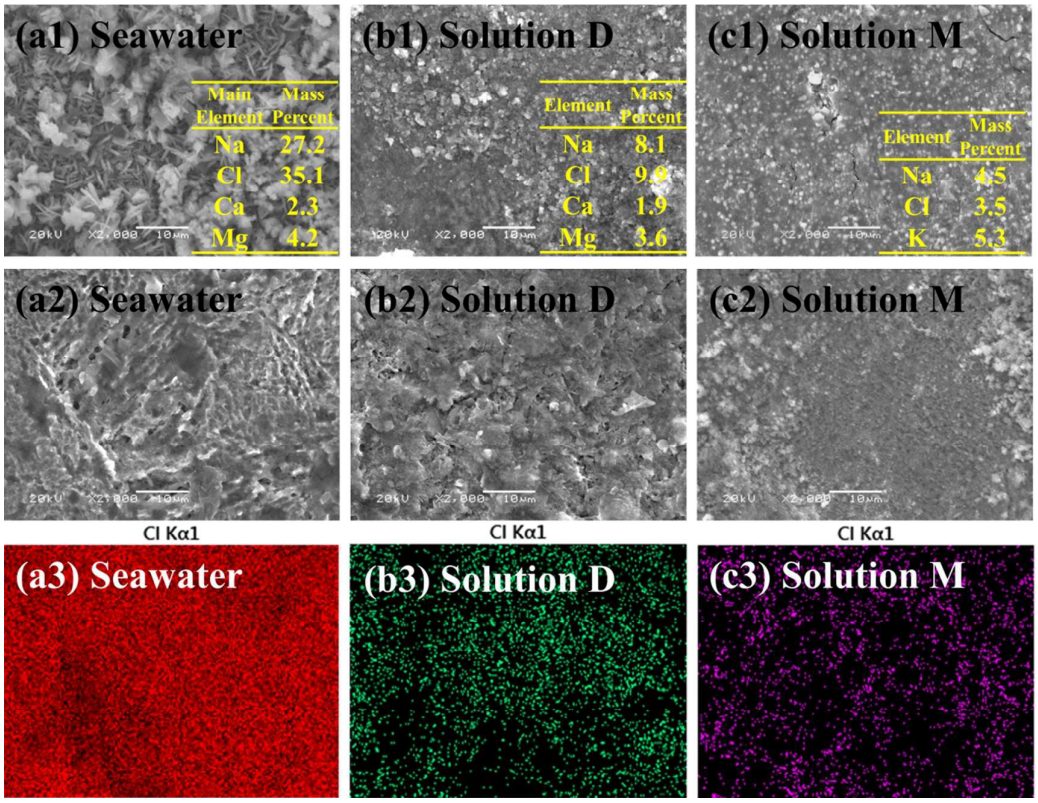

Fig. 17 SEM images of sample surfaces (a1-c1) and corroded surfaces (a2-c2) of bearing steel after immersed in seawater, solution D and solution M, and elemental mapping of Cl on the corroded surface generated in the three solutions (a3-c3).

Meanwhile, Fig. 17 shows SEM images of the steel surfaces after immersed in the three solutions. In Fig. 17a, large amounts of salts containing Na, Cl, Ca and Mg deposit on the steel surface immersed in seawater. In Figs. 17b1 and c1, the salts on the surface immersed in solutions D and M are obviously fewer. Then, the salts were wiped by cotton gently. Figs. 17a2-c2 gives SEM images of the corroded surfaces. In Fig. 17a2, many corrosion pits and microgrooves form on the corroded surface, due to severe seawater corrosion. Furthermore, the elemental mapping shows that the content of Cl on the corroded surface in seawater is much higher than that in the other two solutions (Figs. 17a3-c3). The high concentration of Cl^- in seawater is responsible for the severely corroded surface of steel.

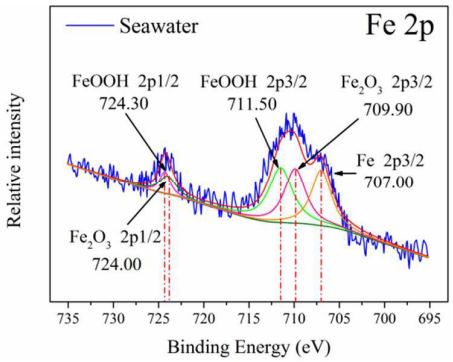

Fig. 18 XPS spectrum of Fe on the corroded surface after immersed in seawater.

Fig. 18 gives XPS spectrum of Fe on the corroded surface immersed in seawater. The peaks at 724.30 eV (Fe 2p 1/2) and 711.50 eV (Fe 2p 3/2) are assigned to FeOOH.[67] The peaks at 724.00 (Fe 2p 1/2) and 709.90 eV (Fe 2p 3/2) are associated with Fe_2O_3.[68] It indicates that the corrosion products on the immersed surface are the same as that on the worn surface.

4. Conclusions

(1) In the four liquids, CANFM alloy exhibits different friction coefficients and wear rates which follow the sequence: seawater < divalent salts solution < monovalent salts solution < distilled water. The friction and wear of CANFM alloy in seawater and divalent salts solution are milder than that in distilled water and monovalent salts solution;

(2) The distribution of $CaCO_3$ and $Mg(OH)_2$ on the surfaces of CANFM alloy and steel can reduce the friction coefficient and wear rate;

(3) In seawater, the Cl^- and SO_4^{2-} adsorbed by surface can accelerate corrosion and promote the formation of Cu_2O, Al_2O_3, FeOOH and Fe_2O_3, which can affect the tribological performances;

(4) Many substances transfer from CANFM alloy to the steel surface, and form

the transfer layer.

(5) During the immersion corrosion tests, the surfaces of CANFM alloy and steel strongly adsorb various ions. In seawater, the high concentration of Cl^- adsorbed on the surface is responsible for the severely corroded surface.

Acknowledgements

This work was supported by the National Natural Science Foundation of China (51202258, 51303188). One of the authors (Zhuhui Qiao) gratefully appreciates the support of State Key Laboratory of Rare Earth on Advanced Materials and Valuable Utilization of Resources, Changchun Institute of Applied Chemistry (RERU2014008).

References

1. S. Kumari, A. Kumar, A. P. Singh, M. Garg, P. K. Dutta, S. K. Dhawan and R. B. Mathur, *RSC Advances*, 2014, **4**, 23202.
2. A. Cao, G. Liu, Y. Yue, L. Zhang and Y. Liu, *RSC Adv.*, 2015, **5**, 58804-58812.
3. A. Al-Hashem and W. Riad, *Materials Characterization*, 2002, **48**, 37-41.
4. C. H. Tang, F. T. Cheng and H. C. Man, *Materials Science and Engineering: A*, 2004, **373**, 195-203.
5. D. R. Ni, P. Xue, D. Wang, B. L. Xiao and Z. Y. Ma, *Materials Science and Engineering: A*, 2009, **524**, 119-128.
6. G. Kear, B. D. Barker, K. Stokes and F. C. Walsh, *Journal of Applied Electrochemistry*, 2004, **34**, 1235-1240.
7. R. C. Barik, J. A. Wharton, R. J. K. Wood, K. S. Tan and K. R. Stokes, *Wear*, 2005, **259**, 230-242.
8. C. H. Tang, F. T. Cheng and H. C. Man, *Surface and Coatings Technology*, 2006, **200**, 2594-2601.
9. Y. Zhou, S. Xu, L. Guo, S. Zhang, H. Lu, Y. Gong and F. Gao, *RSC Adv.*, 2015, **5**, 14804-14813.
10. M. A. Deyab, R. Essehli and B. El Bali, *RSC Adv.*, 2015, **5**, 64326-64334.
11. L. Guo, W. Dong and S. Zhang, *RSC Adv.*, 2014, **4**, 41956-41967.
12. Z. Chai, Y. Liu, J. Li, X. Lu and D. He, *RSC Adv.*, 2014, **4**, 50503-50509.

13. J. Li, Z. Yang, T. Wang, N. Yu, L. Sun, C. Nie, H. Teng, C. Jin, X. Chen and H. Geng, *RSC Adv.*, 2015, **5**, 75044-75054.
14. W. Liang, X. L. Xu, J. J. Xu and Z. K. Hei, *Thin Solid Films*, 2000, **376**, 159-163.
15. V. Barabash, A. Pokrovsky and S. Fabritsiev, *Journal of Nuclear Materials*, 2007, **367-370**, 1305-1311.
16. H. Wu, Q. Bi, S. Zhu, J. Yang and W. Liu, *Tribology International*, 2011, **44**, 1161-1167.
17. Y. Zhang, H. Tang, X. Ji, C. Li, L. Chen, D. Zhang, X. Yang and H. Zhang, *RSC Advances*, 2013, **3**, 26086.
18. G. Cui, Q. Bi, S. Zhu, J. Yang and W. Liu, *Tribology International*, 2012, **55**, 126-134.
19. G. Cui, Q. Bi, S. Zhu, J. Yang and W. Liu, *Tribology International*, 2012, **53**, 76-86.
20. J. Wang, F. Yan and Q. Xue, *Wear*, 2009, **267**, 1634-1641.
21. B. Chen, J. Wang and F. Yan, *Tribology Letters*, 2011, **42**, 17-25.
22. D. R. Ni, B. L. Xiao, Z. Y. Ma, Y. X. Qiao and Y. G. Zheng, *Corrosion Science*, 2010, **52**, 1610-1617.
23. G. Kear, B. D. Barker, K. Stokes and F. C. Walsh, *Journal of Applied Electrochemistry*, 2004, **34**, 1241-1248.
24. M. K. Lee, S. M. Hong, G. H. Kim, K. H. Kim and W. W. Kim, *Metals and Materials International*, 2004, **10**, 313-319.
25. T. Y. A. Sosulnikov M.I., *Doklady AN SSSR*, 1991, **317**, 418.
26. M. D. Demri B., *J. Mater. Process. Technol.*, 1995, **55**.
27. K. M. Haycock D.E., Nicholls C.J., Urch D.S., *J. Chem. Soc. Dalton Trans.*, 1978.
28. H. Karoui, B. Riffault, M. Jeannin, A. Kahoul, O. Gil, M. Ben Amor and M. M. Tlili, *Desalination*, 2013, **311**, 234-240.
29. S. Leon, *Wear* 1983, 207-209.
30. Y. Wang, X. Zhang, J. Liu, Y. Wang, D. Duan and C. Fan, *Materials Science in Semiconductor Processing*, 2015, **40**, 613-620.
31. G. G. G. Jolley J.G., Haukins M.R., Write R.B., Wichlacz P.L., *Appl. Surf. Sci.*, 1989, **37**.
32. J. A. Wharton and K. R. Stokes, *Electrochimica Acta*, 2008, **53**, 2463-2473.
33. B. M. Robert T., Offergeld G., *Surf. Sci.*, 1972, **33**.
34. G. Kear, B. D. Barker and F. C. Walsh, *Corrosion Science*, 2004, **46**, 109-135.
35. Z. Wu, Y. F. Cheng, L. Liu, W. Lv and W. Hu, *Corrosion Science*, 2015, **98**, 260-270.
36. M. D. Collings, D. M. Sherman and K. V. Ragnarsdottir, *Chem. Geol.*, 2000, **167**, 65-73.
37. P. Frank, M. Benfatto, R. K. Szilagyi, P. D'Angelo, S. Della Longa and K. O. Hodgson, *Inorg. Chem.*, 2007, **46**, 7684-7684.
38. J. Eysseltova, V. Zbranek and J. Jirsak, *Collect. Czech. Chem. Commun.*, 1999, **64**, 1262-1268.

39. Q. Zhou, D. Zeng and W. Voigt, *Fluid Phase Equilibria*, 2012, **322-323**, 30-40.
40. H. Huang, Z. Dong, Z. Chen and X. Guo, *Corrosion Science*, 2011, **53**, 1230-1236.
41. Y. Zhou, J. Chen, Y. Xu and Z. Liu, *Journal of Materials Science & Technology*, 2013, **29**, 168-174.
42. M. Asscher, *Surface Science*, 2009, **603**, 957-960.
43. E. Emmez, J. Anibal Boscoboinik, S. Tenney, P. Sutter, S. Shaikhutdinov and H.-J. Freund, *Surface Science*, 2015, DOI: 10.1016/j.susc.2015.06.019.
44. K. D. Danov, P. A. Kralchevsky, G. M. Radulova, E. S. Basheva, S. D. Stoyanov and E. G. Pelan, *Advances in Colloid and Interface Science*, 2015, **222**, 148-161.
45. H. Tao, Y. He and X. Zhao, *Powder Technology*, 2015, **283**, 308-314.
46. Z. K. Ghouri, N. A. M. Barakat, A.-M. Alam, M. S. Alsoufi, T. M. Bawazeer, A. F. Mohamed and H. Y. Kim, *Electrochimica Acta*, 2015, **184**, 193-202.
47. S. K. Park, T. K. Yun, J. Y. Bae and Y. S. Won, *Applied Surface Science*, 2013, **285**, 789-794.
48. D. Milcius, J. Grbović-Novaković, R. Zostautienė, M. Lelis, D. Girdzevicius and M. Urbonavicius, *Journal of Alloys and Compounds*, 2015, **647**, 790-796.
49. P. Ghods, O. B. Isgor, J. R. Brown, F. Bensebaa and D. Kingston, *Applied Surface Science*, 2011, **257**, 4669-4677.
50. S. Montecinos and S. N. Simison, *Applied Surface Science*, 2011, **257**, 7732-7738.
51. H. Gao, J. Zhang, M. Li, K. Liu, D. Guo and Y. Zhang, *Current Applied Physics*, 2013, **13**, 935-939.
52. R. L. Frost, *Spectrochimica Acta Part A: Molecular and Biomolecular Spectroscopy*, 2003, **59**, 1195-1204.
53. F. Dubois, C. Mendibide, T. Pagnier, F. Perrard and C. Duret, *Corrosion Science*, 2008, **50**, 3401-3409.
54. X. Zhang, K. Xiao, C. Dong, J. Wu, X. Li and Y. Huang, *Engineering Failure Analysis*, 2011, **18**, 1981-1989.
55. W. C. Baek, T. Kang, H. J. Sohn and Y. T. Kho, *Electrochimica Acta*, 2001, **46**, 2321-2325.
56. D.-W. Kim and K.-W. Kim, *Wear*, 2013, **297**, 722-730.
57. R. Sánchez-Tovar, R. Leiva-García and J. García-Antón, *Thin Solid Films*, 2015, **576**, 1-10.
58. M. M. Rahman and A. M. Asiri, *Sensing and Bio-Sensing Research*, 2015, **4**, 109-117.
59. N. Garg, S. Bera, G. Mangamma, V. K. Mittal, R. Krishnan and S. Velmurugan, *Surface and Coatings Technology*, 2014, **258**, 597-604.
60. Q. Qu, Y. He, L. Wang, H. Xu, L. Li, Y. Chen and Z. Ding, *Corrosion Science*, 2015, **91**, 321-329.
61. F. Nan, Y. Xu, B. Xu, F. Gao, Y. Wu and X. Tang, *Applied Surface Science*, 2014, **307**, 86-91.

62. N. K. a. E. M. GERARD THOMPSON, *Chemical Engineering Science*, **38**, 1901-1908.
63. Z. Shi, Y. Sun, A. Bloyce and T. Bell, *Wear*, 1996, **193**, 235-241.
64. W. Ma and J. Lu, *Wear*, 2011, **270**, 218-229.
65. D. A. Rigney, *Wear*, 2000, **245**, 1-9.
66. I. Iatsunskyi, M. Kempiński, M. Jancelewicz, K. Załęski, S. Jurga and V. Smyntyna, *Vacuum*, 2015, **113**, 52-58.
67. S. A.G., *Appl. Surf. Sci.*, 1994, **74**.
68. K. K. J. Tan B.J., Sherwood P.M.A., *Chem. Mater.*, 1990, **2**.